

ARTICLE

OPEN



Stronger decadal variability of the Kuroshio Extension under simulated future climate change

Youngji Joh^{1,2}✉, Thomas L. Delworth¹, Andrew T. Wittenberg¹, William F. Cooke¹, Anthony J. Rosati^{2,3} and Liping Zhang^{1,2}

Understanding the behavior of western boundary current systems is crucial for predictions of biogeochemical cycles, fisheries, and basin-scale climate modes over the midlatitude oceans. Studies indicate that anthropogenic climate change induces structural changes in the Kuroshio Extension (KE) system, including a northward migration of its oceanic jet. However, changes in the KE temporal variability remain unclear. Using large ensembles of a global coupled climate model, we show that in response to increasing greenhouse gases, the time scale of KE sea surface height (SSH) shifts from interannual scales toward decadal and longer scales. We attribute this increased low-frequency KE variability to enhanced mid-latitude oceanic Rossby wave activity induced by regional and remote atmospheric forcing, due to a poleward shift of midlatitude surface westerly with climatology and an increase in the tropical precipitation activity, which lead to stronger atmospheric teleconnections from El Niño to the midlatitude Pacific and the KE region. Greenhouse warming leads to both a positive (elongated) KE state that restricts ocean perturbations (e.g., eddy activity) and stronger wind-driven KE fluctuations, which enhances the contributions of decadal KE modulations relative to short-time scale intrinsic oceanic KE variations. Our spectral analyses suggest that anthropogenic forcing may alter the future predictability of the KE system.

npj Climate and Atmospheric Science (2022) 5:63; <https://doi.org/10.1038/s41612-022-00285-z>

INTRODUCTION

The Kuroshio Extension (KE) is an eastward inertial meandering jet of the Kuroshio current located east of Japan, exhibiting the largest air-sea fluxes and the strongest mesoscale eddy activity across the North Pacific basin^{1,2}. The KE is a major part of the Pacific western boundary currents (WBCs) system that transports substantial heat from the tropics to midlatitudes and subsequently releases most of that heat to the atmosphere via turbulent fluxes of latent and sensible heat³. The strongly coupled KE system dynamically interacts with the extratropical Pacific storm track as a midlatitude oceanic frontal zone^{4–7} and, in turn, further impacts large-scale climate modes over the midlatitude Pacific^{8–12}.

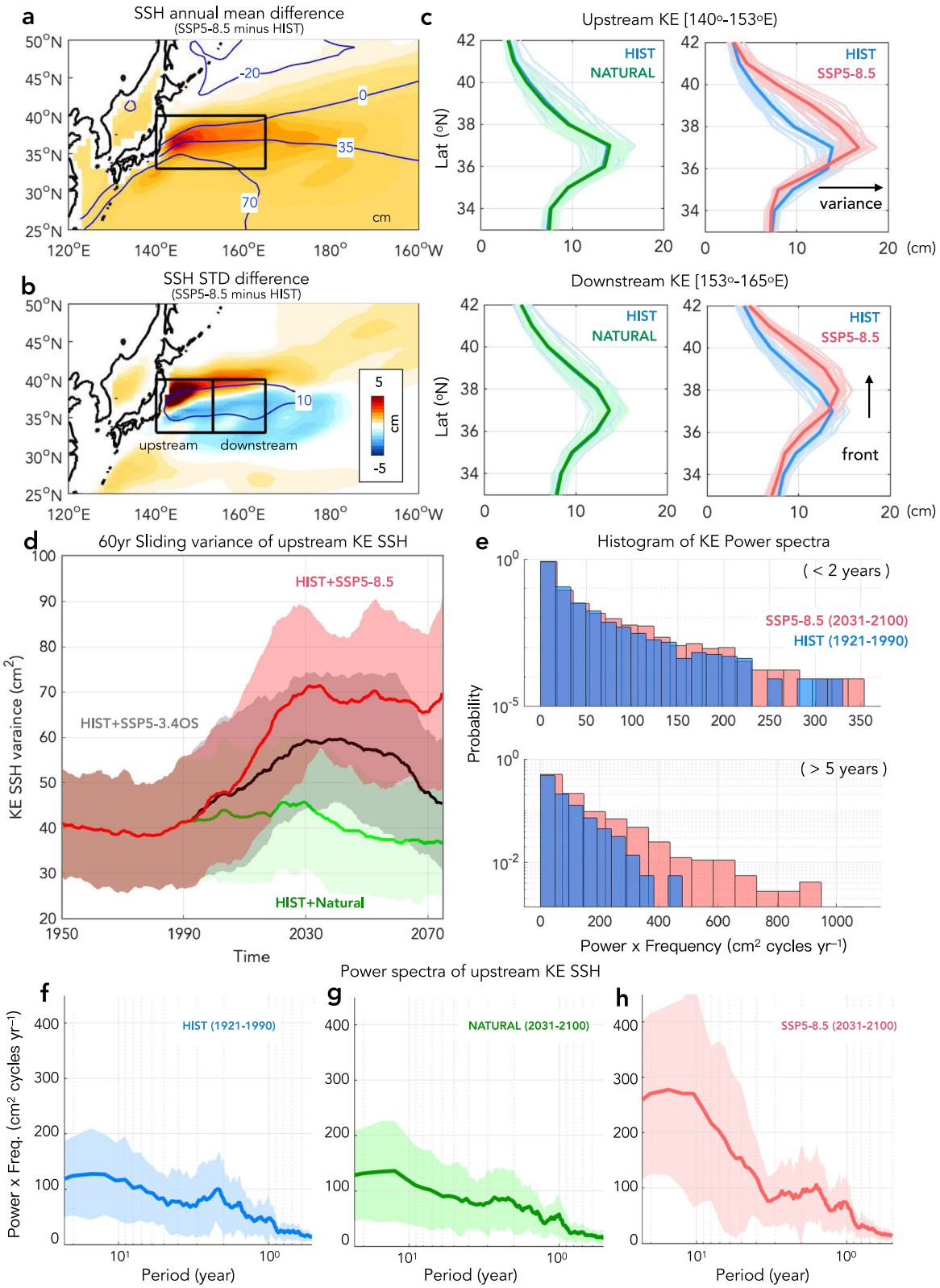
Pacific sea surface height (SSH) variability is most prominent in the KE region [33°–40°N, 140°–165°E] (black box in Fig. 1a) on seasonal-to-decadal timescales. Changes in the eddy kinetic energy (EKE) field over the upstream [140°–153°E] KE region (left box in Fig. 1b) largely contribute to the seasonal-to-interannual time scales of KE variability^{13,14}. This short-time scale KE variation is strongly linked to oceanic intrinsic nonlinearities, characterized by an apparent bimodality^{3,15–18}. The bimodal KE fluctuations include an *elongated state*, when the EKE level *decreases* and the KE jet is relatively straight and stable, and a *contracted state*, in which the EKE *increases* with a spatially convoluted KE path and large meanders^{19,20}. EKE changes are mainly caused by oceanic instability regarding the internal adjustment via the convergence of eddy heat flux and also non-linear interactions of the strong current and eddies²¹. In contrast, basin-wide wind changes over the midlatitudes are the primary forcing of the decadal variability of KE SSH fluctuations^{2,10,20,22–26}. Specifically, atmospheric forcing associated with the North Pacific internal variability, which is also largely associated with El Niño and Southern Oscillation (ENSO) atmospheric teleconnections and their imprints on the “redness” of the spectrum^{27,28}, drives oceanic baroclinic adjustment that

carries wind-induced oceanic Rossby waves westwards towards the WBCs, especially the downstream [153°–165°E] KE region (right box in Fig. 1b)^{2,10,20,22–26}. Oceanic Rossby waves are also closely linked to low-frequency variations in the southern recirculation gyre intensity and the latitudinal migration of the KE jet^{2,13,20,29}. Satellite altimeter measurements and eddy-resolving ocean simulations have shown that the *positive* KE state (e.g., *above-normal* KE SSH anomalies) is accompanied by a *strengthened* southern recirculation gyre and a *northward-displaced* zonal-mean KE path²⁹.

Large-scale oceanic Rossby waves modulate not only the physical characteristics of the WBCs but also the local eddy activity of the KE^{13,14,20,25,30,31}. Interactions between the wind-forced and intrinsic eddy variability in eddy-resolving hindcast simulations reveal that the positive (negative) KE state can be described as the elongated (contracted) state, where the internal ocean perturbations are restricted (favored)^{15,29}. The forced and intrinsic KE variability vary in their respective contributions to the total signal over time^{32,33}. Since the mid-1980s, the decadal modulation of the KE variability has become more robust and prominent³⁴. Given that the dominant forcing of the KE dynamics modulates KE temporal behavior, the relative impact of the oceanic (i.e., intrinsic) versus atmospheric (i.e., forced) drivers on the KE region could be a key source of predictability for KE variability.

Model studies suggest that global warming is associated with intensification and/or a poleward shift of the KE jet in conjunction with systematic changes in wind stress, ocean stratification, and the southern recirculation gyre over the midlatitude Pacific^{35–40}. While these many studies have documented the response of spatial characteristics of the KE system to a warming climate, future temporal changes in the KE variability remain uncertain.

¹Atmospheric and Oceanic Sciences Program, Princeton University, Princeton, NJ, USA. ²Geophysical Fluid Dynamics Laboratory/NOAA, 201 Forrestal Road, Princeton, NJ, USA.
³University Corporation for Atmospheric Research, Boulder, CO, USA. ✉email: youngji.joh@princeton.edu



Here we use Geophysical Fluid Dynamics Laboratory (GFDL) SPEAR (Seamless System for Prediction and EAarth System Research) ensembles of simulations that cover the historical (1921–2014) and future (2015–2100) epochs and investigate the contributions of anthropogenic forcing to the dominant time scale of the KE variability (see Methods for details). The historical

simulation (HIST) is compared with three additional simulations. The first (NATURAL) of these is driven only by changes in natural forcing (solar irradiance and volcanic aerosols) and has anthropogenic forcing fixed at 1921 levels. The second (SSP5-8.5) is an extended simulation of the HIST simulation after 2014, driven by increasing atmospheric greenhouse gas concentrations

Fig. 1 Projected response of spatial and temporal characteristics of Kuroshio Extension SSH variability to future radiative forcing. Difference maps (shading) of North Pacific SSH climatology (**a**) and standard deviation (**b**) between the SSP5-8.5 and HIST large ensemble simulations compared to those from HIST (contour). The black box [33°–40°N, 140°–165°E] in **a** is the KE region defined in this study. **c** A comparison of the standard deviation and ocean front position of the zonally averaged [140°–165°E] KE SSH anomalies between HIST and NATURAL (left column) and SSP5-8.5 (right column) ensemble runs, where the thick dark lines represent the ensemble mean and the thin light lines denote individual ensemble members. **d** 60-year sliding variance of upstream KE SSH [140°–153°E] in HIST + NATURAL (green), HIST + SSP5-8.5 (pink), and HIST + SSP5-3.4OS (gray) ensemble simulations. The moving windows are computed by skipping a month. The solid line represents the ensemble mean and the shading indicates a 90% confidence interval based on the Bootstrapping test (see Methods). **e** Histograms of KE SSH power spectra for the periods for 70 epochs from the HIST (blue, 1921–1990) and SSP5-8.5 (pink, 2031–2100), where the short-time (<2 years) and longer-time (>5 years) scales of Power spectra histograms are separately shown in top and bottom panel, respectively. Power spectra of upstream KE SSH for the periods for 70 epochs from HIST (**f**), NATURAL (**g**), and SSP5-8.5 (**h**).

corresponding to the highest projected Shared Socioeconomic Pathway (SSP). The third (SSP5-3.4OS) follows the SSP5-8.5 simulation until 2040, but thereafter is forced by rapidly decreasing greenhouse gas concentrations. SPEAR has been successfully used for climate studies, including seasonal to decadal variability and prediction of the KE⁴¹. Specifically, SPEAR hindcasts realistically capture the temporal evolution of KE SSH variations, with skillful retrospective KE predictions on both seasonal and multiannual time scales. Given SPEAR's reliable simulations of ocean wave propagation and wind-induced KE atmospheric forcing, the present study focuses on the responses of the spatiotemporal evolution of KE variability to the different future scenarios of SPEAR. Our results suggest that an enhanced positive (elongated) state and the corresponding changes in ENSO atmospheric teleconnections lead to an increase in wind-driven decadal KE variability in anthropogenic warming.

RESULTS AND DISCUSSION

Projected future changes in the KE variance

We first confirm that the SPEAR simulation reproduces the spatiotemporal characteristics of historical KE SSH variability in satellite-derived observations. Like most coupled global climate models with relatively low oceanic horizontal resolutions, SPEAR produces a KE jet with excessive overshoot. However, the model reasonably reproduces the observed KE pattern, with a strong frontal SSH signature and KE SSH variance comparable to the observation (Supplementary Fig. 1). Anthropogenic radiative forcing simulations reveal significant spatial changes in both the KE mean state with an intensification of the southern recirculation gyre (Fig. 1a) and poleward shift of the KE front (Fig. 1b) and an increase in SSH variance corresponding to a more positive KE state^{35–40}. The NATURAL simulation closely resembles the HIST simulation (Fig. 1c, left column), while the SSP5-8.5 simulation confirms the significantly altered variance and position of the KE SSH (Fig. 1c, right column), exceeding the range of intrinsic variation represented by the ensemble spread. An increase in SSH variance and a poleward-shift of the KE SSH front appear in the upstream and downstream KE regions, respectively, consistent with the observed changes in recent decades³⁶. The increasing variance is prominent in the northern part of the upstream region [36°–41°N, 140°–153°E]. This substantial increase in upstream KE intensity under the external forcing is shown from 1960 to 2060 (pinks in Fig. 1d). We find that the stronger upstream KE SSH variance in SSP5-8.5 mostly stems from the enhanced variance at longer time scales, as shown in the histograms of spectral power (Fig. 1e). In the spectral analysis of upstream KE SSH (Fig. 1f–h), the power at high frequencies (monthly to interannual) is similar across the simulations, while the power at low frequencies (~>7 years) is considerably stronger in SSP5-8.5 than in the HIST and NATURAL runs, indicating that the proportion of decadal to interannual KE variance significantly increases with increasing greenhouse gas concentrations. In summary, the projected warmer climate leads to the enhanced decadal variance of the KE (which leads to an overall increase in the upstream KE

variance), and the preferred time scales of the upstream KE variability shift from the interannual toward decadal and longer time scales. In contrast, no changes in the variance and temporal variability of upstream KE SSH are detected between the natural forcing and historical run in Fig. 1.

Hypothesis for changes in the KE variance in a warmer climate

Based on established mechanisms of the KE variability^{13,14,20,25,30,31}, a projected future shift in the dominant spectral peak of KE variability from interannual to decadal time scales may be due to changes in contributions of seasonal-to-interannual eddy activity and decadal wind-driven forcing to the total KE variability. Our hypothesis is that the portion of (1) short-lived eddy activity may be limited due to favorable conditions for the positive (elongated) KE state, which favors intensified recirculation gyres and a northward KE jet but restricts internal ocean perturbations, and (2) the role of atmospherically-driven KE fluctuations (e.g., midlatitude oceanic Rossby wave adjustment) may become more significant through enhanced ENSO atmospheric teleconnections as a consequence of changes in the mean background climate and increasing tropical forcing.

We first present changes in mean background wind circulations over the Northwest Pacific (Fig. 2a). A comparison of the HIST and SSP5-8.5 simulations (compare blues and pinks in Fig. 2a) shows an intensification and poleward shift of the near-surface midlatitude westerly wind stress^{35–40}. These produce an anticyclonic wind stress change over the WBCs (Fig. 2b and Supplementary Fig. 2), which can enhance the Ekman convergence into the KE region (pink box), interior southward Sverdrup transport, westward SSH upslope, northward western boundary current, and KE southern recirculation gyre, leading to a positive (elongated) KE state as seen in Fig. 1a, b.

We next show changes in tropical forcing under future climate projections. With increasing greenhouse gas concentrations, Nino3.4 SST anomaly variance strengthens (pink in Fig. 2c), as do the mean and variance of tropical rainfall (Fig. 2d)^{42–46}. We find that a joint impact of the latitudinally-displaced mean background winds (Fig. 2a) with the enhanced remote forcing from the tropics (Fig. 2c) may lead to stronger influences of the ENSO atmospheric teleconnections on large-scale wind forcing of the KE variability (Fig. 3). Changes in ENSO atmospheric teleconnections from the HIST (Fig. 3a) to SSP5-8.5 run (Fig. 3b) show the reinforced quasi-stationary atmospheric waves, inducing stronger basin-scale atmospheric anomalies over the midlatitudes^{2,10,20,23–27}. ENSO's North Pacific teleconnections strengthen and shift northeastward (Fig. 3c), which are probably associated with altered background wind field, driving more significant wind-induced Rossby wave adjustment of the upper ocean over the Central Pacific KE band (pink box in Fig. 3c). The impact of ENSO on the KE SSH considerably increases with external forcing (Fig. 3d). In the warmer climate, the ENSO-induced oceanic Rossby waves propagate westward into the KE region with larger amplitude SSH anomalies (compare Fig. 3e, f). Our results suggest that the upstream KE region, where intrinsic perturbations dominated during the historical epoch, may become increasingly affected by

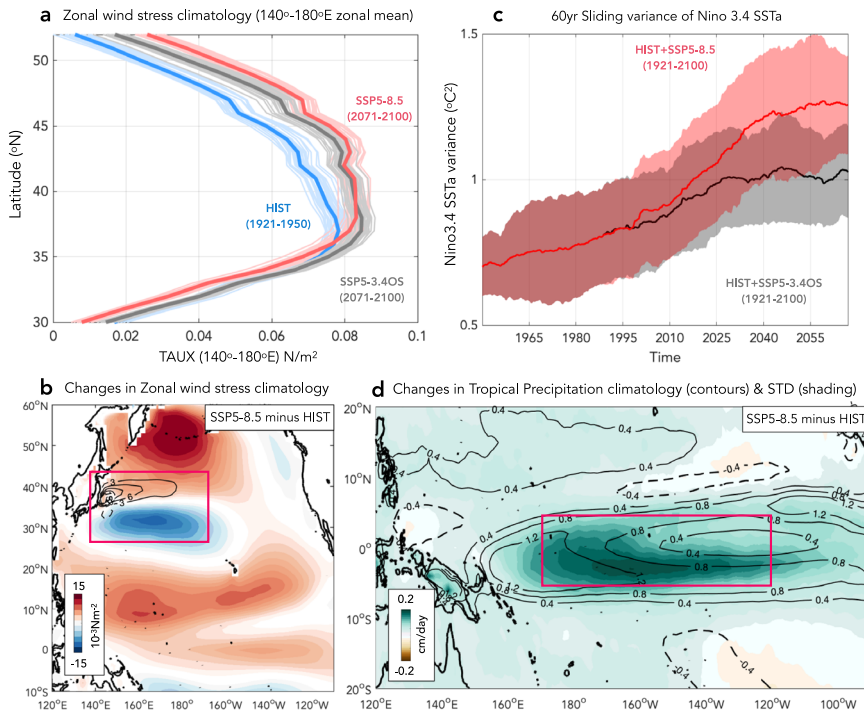


Fig. 2 Climate response to changing greenhouse gas concentrations. **a** Zonal mean surface wind stress of the North Pacific midlatitude over the earlier and later time periods of 30 year epochs from HIST (1921–1950, blue), SSP5-3.4OS (2071–2100, gray), and SSP5-8.5 (2071–2100, pink) runs. Thick lines represent the ensemble mean, and thin lines the individual members. **b** Change in zonal wind stress climatology from HIST to SSP5-8.5. Contours show SSH anomalies regressed on the KE index over the period between 1921–2100. The pink box covering the western boundary current system indicates the zone of intensified Ekman convergence (strengthened anti-cyclonic surface winds). **c** 60-year sliding variance of Nino3.4 SST anomalies ($^{\circ}\text{C}^2$) in HIST + SSP5-8.5 (pink) and HIST + SSP5-3.4OS (gray) ensemble simulations. The moving windows are computed by skipping a month. The solid line represents the ensemble mean and shading indicates a 90% confidence interval based on the Bootstrapping test (see Methods). **d** Changes in annual mean climatology (contours, cm/day) and monthly anomaly standard deviation (shading, cm/day) of the tropical Pacific precipitation from HIST to SSP5-8.5. The pink box denotes the Nino3.4 region [5°S – 5°N , 120° – 170°W].

wind forcing from ENSO. Thus, we attribute the stronger decadal fluctuations over the upstream KE (Fig. 1e) to both enhanced ENSO-driven oceanic forcing and the strengthened and poleward shifted midlatitude climatological westerlies. The ENSO-related KE SSH variability strengthens on decadal timescales from the HIST (Fig. 3g) to SSP5-8.5 (Fig. 3h) run. Changes in the ENSO’s impacts on the KE (Fig. 3i) resemble the changes in North Pacific SSH variability, with an increase in upstream KE intensity and a northward shift of the KE front (compare Figs. 1b and 3i).

We show that a ratio of decadal to interannual KE variance has significantly increased from the HIST to SSP5-8.5 run in the majority (23 of 30) of ensemble members (Fig. 4a and Supplementary Figs. 3–4). The scatterplots using those 23 members confirm that the increasing decadal KE variance is largely driven by changes in the background wind fields (Fig. 4b) and tropical rainfall variability (Fig. 4c). Specifically, the mean KE zonal wind climatology and Nino3.4 precipitation anomaly variance both predict the ratio of decadal to interannual variance of upstream KE SSH, especially in SSP5-8.5 (~35–40%) (Note that *the tropical rainfall variance and the mean zonal wind stress over the KE region are barely dependent in the simulations*). Under anthropogenic climate change, the weakened annual-mean zonal wind stress over the KE region reduces the frontal baroclinicity and may limit eddy activity (e.g., reduced short-time scale KE variance)^{2,32}. The significant relationship between the zonal winds and the KE variance ratio is found in both simulations, but largely increases from the HIST ($R = -0.38$, $p < 0.1$) to the SSP5-8.5 run ($R = -0.61$, $p < 0.05$) in Fig. 4b. On the other hand, the contribution of tropical rainfall activity barely exists in HIST ($R = -0.1$), but substantially increases in SSP5-8.5 ($R = 0.63$, $p < 0.001$). The results

indicate that anthropogenic changes in the midlatitude wind stress climatology and tropical precipitation variance may play an important role in modulating the upstream KE SSH time scales.

Sensitivity of the KE response to radiative forcing

To further examine the sensitivity of response of the KE variability to atmospheric greenhouse gas concentrations, we investigate an additional simulation, SSP5-3.4OS, which resembles SSP5-8.5 until 2040, after which there is a substantial decline in greenhouse gas concentrations^{47,48}. In the SSP5-3.4OS simulation, we note that the KE intensity that had increased with radiative forcing until 2040 (grays in Fig. 1d) immediately responds to the steep greenhouse gas reduction and decreases until 2100. Also, Fig. 4d confirms that the KE total amplitude and a ratio of decadal to interannual KE SSH variance increase with greenhouse gas concentrations and decrease when the greenhouse gases are reduced in the SSP5-3.4OS simulation after 2070. The results indicate that the variance and preferred time scale of KE variability sensitively vary with changing radiative forcing.

To address the sensitivity of KE variability to the external climate driver, we revisit behaviors of the anthropogenic-induced climate feedbacks (e.g., wind stress climatology and Nino3.4 SST variability in Fig. 2) by comparing the SSP5-3.4OS and SSP5-8.5 runs. Figure 2a compares the North Pacific westerlies between the SSP5-8.5 (pink) and SSP5-3.4 OS (gray) for the final 30-year epoch [2071–2100]. The northward-shifted winds climatological westerly winds move back towards their original position as greenhouse gas concentrations decline (grays in Fig. 2a), implying that the poleward displacement of the KE ocean front may be reversible. In contrast, the amplitude of both midlatitude westerlies climatology

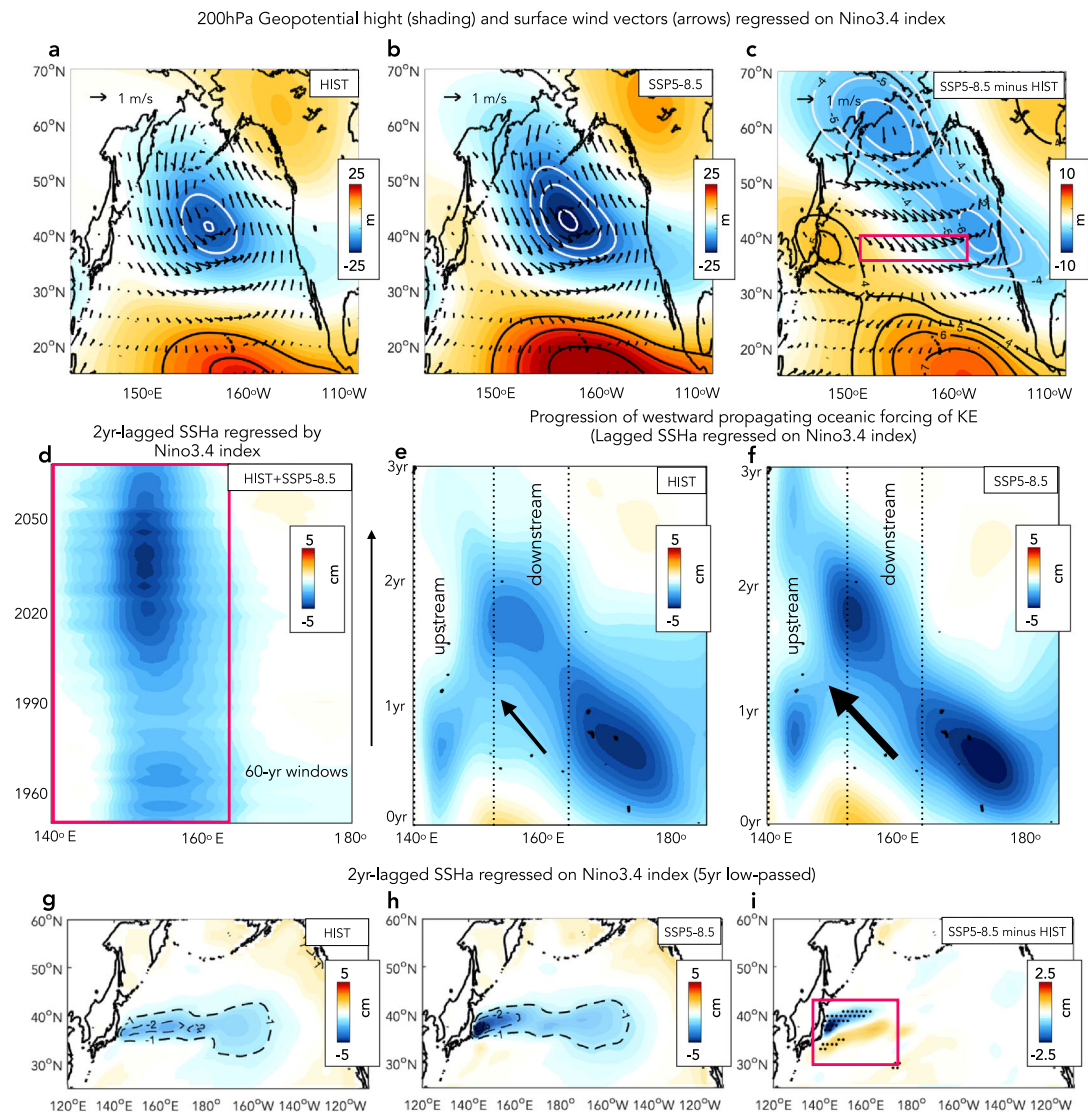


Fig. 3 ENSO teleconnection changes and corresponding impact on wind-driven KE SSH variability. **a–c** 200 hPa geopotential height (unit: m, shading) and surface wind (arrows) anomalies regressed onto the normalized Nino3.4 index from HIST (**a**) and SSP5-8.5 (**b**), and their difference (SSP5-8.5 minus HIST) (**c**). **d** Hovmöller diagrams (cm) of 2yr-lagged KE SSH anomalies (meridionally averaged of 33° – 40° N) regressed onto the normalized Nino3.4 index from the HIST + SSP5-8.5 simulation. The computation is done with overlapping 60-year windows, skipping by 5 years. **e, f** Hovmöller diagrams (cm) of lagged KE SSH anomalies (meridionally averaged of 33° – 40° N region) regressed onto the normalized Nino3.4 index from HIST (**e**) and SSP5-8.5 (**f**). Arrows indicate westward propagations of oceanic Rossby waves. **g–i** 2yr-lagged SSH anomalies regressed onto 5yr-lowpassed Nino3.4 index from HIST (**g**) and SSP5-8.5 (**h**) and their difference map (**i**, SSP5-8.5 minus HIST). The pink box highlights the changes in the ENSO-forced KE oceanic signature from the HIST to SSP5-8.5 run, for comparison with the changes in the North Pacific SSH standard deviation seen in Fig. 1.

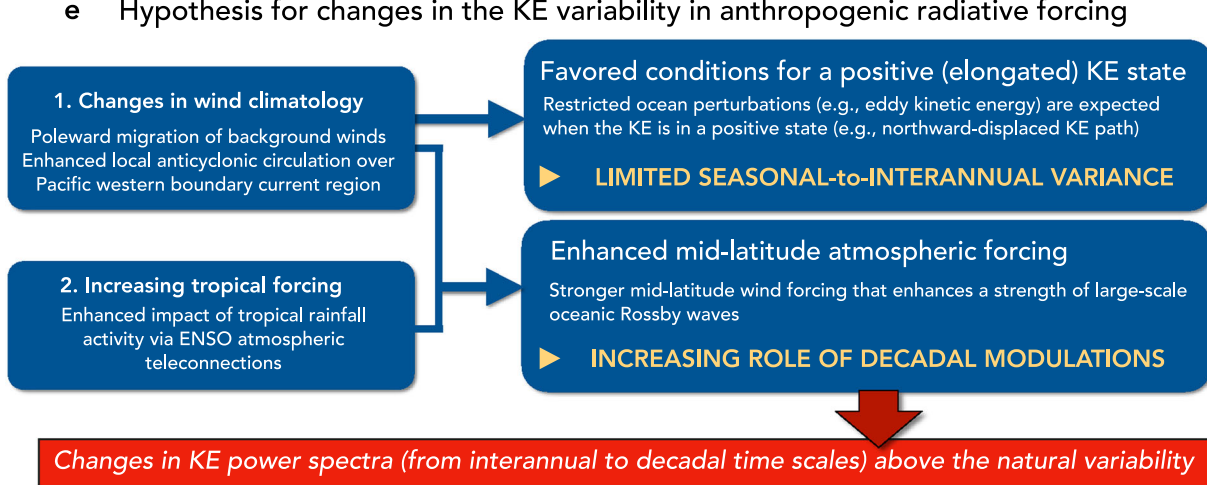
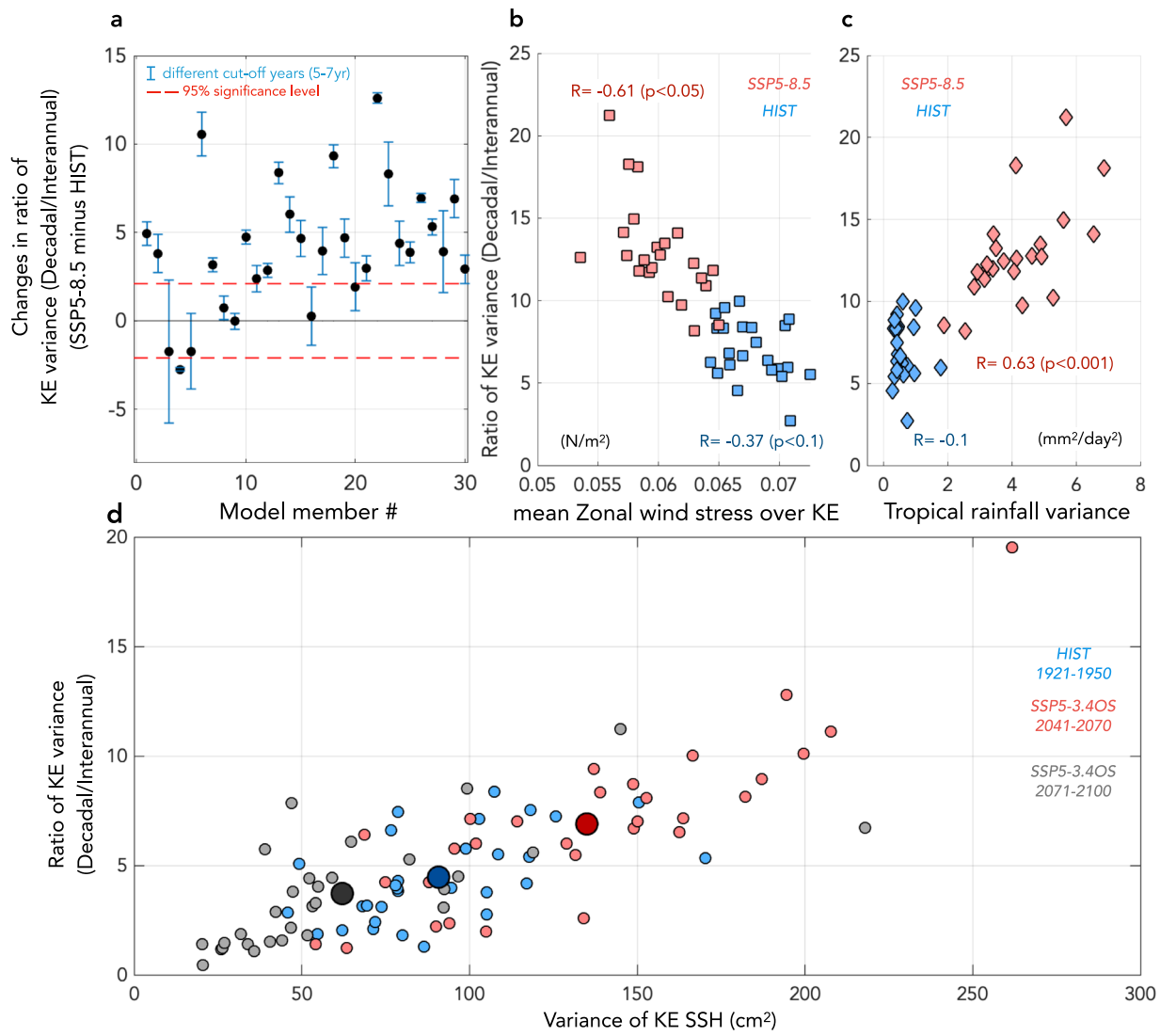
(grays in Fig. 2a) and ENSO (grays in Fig. 2c) remains strong even after the greenhouse gas concentrations are reduced beyond 2040, suggesting that there may be some critical thresholds or hysteresis in the tropical and subtropical Pacific climate system. We suggest that the *altered mean position* (reversible) of surface wind climatology (Fig. 2a) might be a more critical factor than the *enhanced intensity* (irreversible) of tropical SST activity (Fig. 2c) for the variance and dominant time scale of KE variability.

Summary and implications

Using different radiative forcing scenarios, we show that the KE preferred timescale varies with changing greenhouse gas concentrations, and its decadal variability significantly increases with anthropogenic radiative forcing. Our findings suggest that anthropogenic-forced changes in surface wind climatology favor the positive (elongated) KE mean state and make the upstream KE

SSH more stable, which may restrict the role of upstream eddy activity^{13,14,20,25,30,31}, leading to a reduced contribution of seasonal-to-interannual intrinsic variability to the total KE. The joint influences of poleward-displaced mean background winds and enhanced tropical convective forcing may lead the wind-driven decadal variability to become dominant in the upstream KE region. Together, the greenhouse gases weaken the seasonal-to-interannual oceanic intrinsic KE variability while amplifying the wind-forced decadal KE variability (Fig. 4e).

The large-ensemble analysis adopted in this study demonstrates significant and robust contributions of anthropogenic warming to projected changes in the KE system beyond the uncertainty arising from internal climate variability. One may raise doubts whether the above findings would be constrained by the relatively coarse ocean model resolution (1°) used in this study, which might underestimate intrinsic oceanic processes such as



mesoscale eddy activity. It is true that the current configuration of SPEAR cannot fully resolve small-scale ocean dynamics. However, we stress the evident changes in the local and remote atmospheric forcing in a warming climate, which have been extensively demonstrated as the key drivers of KE modulations

from satellite altimeter observations and ocean model experiments^{13,14,20,25,30,31}. Moreover, the projected KE variability from this study is highly supported by ongoing climate changes, such as the northward shifted downstream KE jet^{36,49} and the more prominent decadal KE variability during the recent decades³⁴.

Fig. 4 Changes in ratio of KE variance, and their hypothesized linkages to anthropogenically-induced climate changes. **a** Changes in the ratio of KE variance (y-axis) from HIST (1921–1990) to SSP5-8.5 (2031–2100), computed as the decadal KE variance (mean spectral power over the periods > cut-off year) divided by interannual KE variance (mean spectral power over the periods < cut-off year). Different cut-off years (5–7 years) are used to define decadal/interannual time scales. The red dashed lines denote where the changes in decadal/interannual ratio between two periods are significant. Error bars indicate ratio ranges of using cut-off years and black dots denote the mean in each individual ensemble. Statistically significant relationships of the ratio of KE variance for 70-year epoch in **a** between the mean zonal wind stress (**b**) over the KE band [140°E – 180° & 30° – 36°N] and Nino3.4 precipitation variability (**c**) for 1921–1940 from HIST (blue) and 2081–2100 from SSP5-8.5 (pink). In the scatter diagrams, 23 members showing significant changes above the significance level in **a** are used. **d** Increasing KE SSH total variance and the ratio of KE variance (decadal/interannual) with rising anthropogenic forcing in HIST and SSP5-3.4OS large ensemble simulations. Blues denote periods of the HIST run and pinks and grays indicate periods corresponding to increasing and decreasing radiative forcing in the SSP5-3.4OS run, respectively. The large circles indicate the means of the colored periods. **e** Schematic showing how the two main drivers associated with anthropogenically-induced climate changes could affect the time scales of KE variability.

Given the significant contributions of midlatitude atmospheric variability to the air-sea coupled KE dynamics and their changes, our findings may also suggest a role for changes in mesoscale oceanic eddy activity, via their known interactions with basin-scale atmospheric/oceanic circulations^{13,14,20,25,29–31}.

The future changes in the spatiotemporal patterns of KE variability have implications for both regional and large-scale climate change. A poleward shift in the KE front may alter the KE-induced surface wind anomalies over the North Pacific by modulating the path of the storm track^{4–7} and the large-scale atmospheric/oceanic circulations^{8–12}. Also, a link between the mechanisms of the WBC system and the North Pacific subtropical mode water^{36,50} suggests possible changes in the formation or subduction rate of the mode water, which play a key role in the biological pump and ocean carbon sinks in the Northern Hemisphere. Thus, an important remaining question is to what extent changes in the KE system would impact the regional downstream feedback or large-scale North Pacific climate in the future. Increasing decadal variability of the KE might amplify extreme events and threats to ecosystems^{51,52}, while also possibly lending improved decadal predictability to the Pacific climate.

METHODS

Datasets

The model used in this study is the SPEAR (Seamless System for Prediction and Earth System Research) model⁵³, a newly developed atmosphere and ocean fully coupled model at the NOAA Geophysical Fluid Dynamics Laboratory (GFDL). We use an ensemble of historical runs (labeled “HIST”) that cover 1921–2014 as a base period, where all radiative forcings and land cover from both human and natural sources are incorporated, including greenhouse gases, aerosols, ozone, solar irradiance, and volcanic aerosols. We then compare the historical KE characteristics with those from ensembles of three different future runs that cover 2015–2100. In the first suite of future simulations (labeled “Natural”), the run is simulated with only natural forcing, where solar irradiance and volcanic aerosols vary as projected, but anthropogenic forcing is fixed at the 1921 levels. The second ensemble suite is a projection for a Shared Socioeconomic Pathway (SSP) covering the 2015–2100 time period^{54,55}. We use the highest radiative forcing scenario (labeled as “SSP5-8.5”). To investigate the sensitivity and potential reversibility of the KE response to the prescribed atmospheric concentrations of greenhouse gases, we compare the results from the Natural and SSP5-8.5 simulations to the overshoot scenario (SSP5-3.4OS). In the SSP5-3.4OS experiment, the greenhouse gas concentration increases until 2040 following the SSP5-8.5 radiative forcing, and rapidly decreases thereafter. In each of the three experiments, 30 ensemble members are conducted. Utilizing the large ensemble size, we compare the impact of external forcing with the uncertainty arising from internal climate variability. Anomalies for the variables and the removal of the warming trend are obtained by subtracting the ensemble-mean of temporal smoothing of the seasonal climatology from the individual ensemble members. More details about the SPEAR ensemble run can be found in Delworth et al. (2020)⁵³.

Definition of indices

The oceanic KE index is computed as area-averaged sea surface height anomalies over the KE region [33° – 40°N , 140° – 165°E], where the strongest SSH standard deviation is detected in the coupled model. The KE region defined in this study is slightly different from the previous studies (e.g., [31° – 36°N , 140° – 165°E], Qiu et al. 2014) because the latitudinal position of the KE jet in our coupled models is displaced north of the observations, as is the case in most global coupled climate models with insufficient ocean resolution⁵⁵. The upstream and downstream regions in Fig. 1b, c are defined as [140° – 153°E] and [153° – 165°E] respectively^{21,31}. Changes in the upstream region KE variance in Fig. 1c are localized to [35° – 41°N], so the power spectra of upstream KE are calculated for [35° – 39°N , 140° – 153°E] for HIST and [36° – 40°N , 140° – 153°E] for SSP5-8.5. For the ENSO index, we use sea surface temperature anomalies in the Nino3.4 region [5°S – 5°N , 120° – 170°W].

Confidence interval for a sliding variance

We use a bootstrap method to show the uncertainty in the KE and ENSO variance among different ensemble members (Figs. 1d and 2c). The bootstrap method involves iteratively resampling the data with replacement. In each sliding window, 30-member pseudo-ensembles are drawn randomly (with replacement) from among the actual 30-member ensemble and used to compute the ensemble-mean temporal variance of the KE and ENSO. This procedure is repeated 10,000 times, resulting in a bootstrap-sampled Probability Density Function of ensemble-mean temporal variances, whose 10th and 90th percentiles are plotted as the shading in Figs. 1d and 2c.

Spectral power analysis

Power spectra of KE SSH are computed by the power times frequency (cycles year⁻¹) as a function of the period (year) based on a forward Fast Fourier Transform. The interannual and decadal timescales in this study are determined by using a cut-off time of 7 years (Fig. 4b–d). However, our results are not dependent on the selection of the cut-off time scales between 5–7 years as shown in Fig. 4a.

Sensitivity of changes in the KE to radiative scenarios

For each future projection, a 30-member ensemble was simulated and used in the analysis. 28 of the 30 ensemble members (93%) show increased upstream KE intensity, and 23 of the 30 ensemble members (77%) indicate significantly strengthened decadal KE variance from the HIST to SSP5-8.5 radiative forcing simulation across using different cut-off time scales (5–7 years). All ensemble members (100%) show the enhanced tropical precipitation variability and poleward shifted midlatitude climatological westerly winds⁵⁶.

DATA AVAILABILITY

The SPEAR large-ensemble datasets for this paper are available on a ftp server (ftp://data1.gfdl.noaa.gov/users/youngji.joh/kuroshio_changes).

CODE AVAILABILITY

Codes generated during the present study are available from the corresponding author upon request.

Received: 26 January 2022; Accepted: 11 July 2022;
Published online: 02 August 2022

REFERENCES

- Qiu, B. & Kelly, K. A. Upper-ocean heat balance in the Kuroshio Extension region. *J. Phys. Oceanogr.* **23**, 2027–2041 (1993).
- Qiu, B. & Chen, S. Eddy-mean flow interaction in the decadally modulating Kuroshio Extension system. *Deep Sea Res. Part II: Top. Stud. Oceanogr.* **57**, 1098–1110 (2010).
- Kelly, K. A. et al. Western boundary currents and frontal air-sea interaction: gulf stream and Kuroshio Extension. *J. Clim.* **23**, 5644–5667 (2010).
- Nakamura, H., Sampe, T., Goto, A., Ohfuchi, W. & Xie, S.-P. On the importance of midlatitude oceanic frontal zones for the mean state and dominant variability in the tropospheric circulation. *Geophys. Res. Lett.* **35**, <https://doi.org/10.1029/2008gl034010> (2008).
- O'Reilly, C. H. & Czaja, A. The response of the Pacific storm track and atmospheric circulation to Kuroshio Extension variability. *140*, 52–66, <https://doi.org/10.1002/cj.2334> (2015).
- Ma, X. et al. Distant influence of Kuroshio Eddies on North Pacific weather patterns? *Sci. Rep.* **5**, 17785 (2015).
- Small, R. J., Tomas, R. A. & Bryan, F. O. Storm track response to ocean fronts in a global high-resolution climate model. *Clim. Dyn.* **43**, 805–828 (2014).
- Latif, M. & Barnett, T. P. Casues of decadal climate variability over the North Pacific and North America. *Science* **266**, 634–637 (1994).
- Latif, M. & Barnett, T. P. Decadal Climate variability over the North Pacific and North America: dynamics and predictability. *J. Clim.* **9**, 2407–2423 (1996).
- Kwon, Y.-O. et al. Role of the Gulf Stream and Kuroshio-Oyashio systems in large-scale atmosphere–ocean interaction: a review. *J. Clim.* **23**, 3249–3281 (2010).
- Frankignoul, C., Sennéchal, N., Kwon, Y.-O. & Alexander, M. A. Influence of the meridional shifts of the Kuroshio and the Oyashio extensions on the atmospheric circulation. *J. Clim.* **24**, 762–777 (2011).
- Joh, Y. & Di Lorenzo, E. Interactions between Kuroshio Extension and Central Tropical Pacific lead to preferred decadal-timescale oscillations in Pacific climate. *Sci. Rep.* **9**, <https://doi.org/10.1038/s41598-019-49927-y> (2019).
- Taguchi, B. et al. Decadal variability of the Kuroshio Extension: mesoscale eddies and recirculations. *Ocean Dyn.* **60**, 673–691 (2010).
- Qiu, B. & Chen, S. Effect of Decadal Kuroshio Extension Jet and Eddy variability on the modification of north pacific intermediate water. *J. Phys. Oceanogr.* **41**, 503–515 (2011).
- Qiu, B. Interannual Variability of the Kuroshio Extension system and its impact of the wintertime SST field. *J. Phys. Oceanogr.* **30**, 1486–1502 (2000).
- Penduff, T. et al. Sea level expression of intrinsic and forced ocean variabilities at interannual time scales. *J. Clim.* **24**, 5652–5670 (2011).
- Sasaki, Y. N. & Minobe, S. Climatological mean features and interannual to decadal variability of ring formations in the Kuroshio Extension region. *J. Oceanogr.* **71**, 499–509 (2015).
- Sérazin, G. et al. Intrinsic variability of sea level from global ocean simulations: spatiotemporal scales. *J. Clim.* **28**, 4279–4292 (2015).
- Qiu, B. Mean flow and variability in the Kuroshio Extension from geosat altimetry data. *J. Geophys. Res.* **96**, 18491–18605 (1991).
- Qiu, B. & Chen, S. Variability of the Kuroshio Extension Jet, recirculation gyre, and mesoscale eddies on decadal time scales. *J. Phys. Oceanogr.* **35**, 2090–2103 (2005).
- Nonaka, M., Sasai, Y., Sasaki, H., Taguchi, B. & Nakamura, H. How potentially predictable are midlatitude ocean currents. *Sci. Rep.* **6**, 20153 (2016).
- Deser, C., Alexander, M. A. & Timlin, M. S. Evidence for a wind-driven intensification on the Kuroshio Current Extension from the 1970s to the 1980s. *J. Clim.* **12**, 1697–1706 (1999).
- Seager, R., Kushnir, Y., Naik, N. H., Cane, M. A. & Miller, J. Wind-driven shifts in the latitude of the Kuroshio-Oyashio Extension and generation of SST anomalies on decadal timescales. *J. oc Clim.* **14**, 4249–4265 (2001).
- Qiu, B. Kuroshio extension variability and forcing of the Pacific decadal oscillations: responses and potential feedback. *J. Phys. Oceanogr.* **33**, 2465–2482 (2003).
- Taguchi, B. et al. Decadal variability of the Kuroshio Extension: Observations and an Eddy-Resolving Model Hindcast. *J. Clim.* **20**, 2357–2377 (2007).
- Ceballos, L. I., Di Lorenzo, E., Hoyos, C. D., Schneider, N. & Taguchi, B. North Pacific Gyre oscillation synchronizes climate fluctuations in the Eastern and Western Boundary Systems. *J. Clim.* **22**, 5163–5174 (2009).
- Trenberth, K. E. et al. Progress during TOGA in understanding and modeling global teleconnections associated with tropical sea surface temperatures. *J. Geophys. Res.-Oceans* **103**, 14291–14324 (1998).
- Alexander, M. A. et al. The atmospheric bridge: the influence of ENSO teleconnections on air-sea interaction over the global oceans. *J. Clim.* **15**, 2205–2231 (2002).
- Qiu, B., Chen, S., Schneider, N. & Taguchi, B. A coupled decadal prediction of the dynamic state of the Kuroshio Extension System. *J. Clim.* **27**, 1751–1764 (2014).
- Taguchi, B., Xie, S.-P., Mitsudera, H. & Kubokawa, A. Response of the Kuroshio Extension to Rossby waves associated with the 1970s climate regime shift in a high-resolution ocean model. *J. Clim.* **18**, 2979–2995 (2005).
- Nonaka, M., Sasaki, H., Taguchi, B. & Nakamura, H. Potential predictability of interannual variability in the Kuroshio Extension jet speed in an eddy-resolving OGCM. *J. Clim.* **25**, 3645–3652 (2012).
- Nonaka, M., Sasaki, H., Taguchi, B. & Schneider, N. Atmospheric-driven and intrinsic interannual-to-decadal variability in the Kuroshio Extension jet and eddy activities. *Front. Mar. Sci.* **7**, <https://doi.org/10.3389/fmars.2020.547442> (2020).
- Qiu, B., Chen, S., Wu, L. & Kida, S. Wind- versus Eddy-forced regional sea level trends and variability in the North Pacific Ocean. *J. Clim.* **28**, 1561–1577 (2015).
- Joh, Y., Di Lorenzo, E., Siqueira, L. & Kirtman, B. P. Enhanced interactions of Kuroshio Extension with tropical Pacific in a changing climate. *Sci. Rep.* **11**, <https://doi.org/10.1038/s41598-021-85582-y> (2021).
- Wu, L. et al. Enhanced warming over the global subtropical western boundary currents. *Nat. Clim. Change* **2**, 161–166 (2012).
- Wu, B., Lin, X. & Yu, L. Poleward Shift of the Kuroshio Extension Front and its impact on the North Pacific subtropical mode water in the recent decades. *J. Phys. Oceanogr.* **51**, 457–474 (2021).
- Yang, H. et al. Intensification and poleward shift of subtropical western boundary currents in a warming climate. *J. Geophys. Res.: Oceans* **121**, 4928–4945 (2016).
- Zhang, X., Wang, Q. & Mu, M. The impact of global warming on Kuroshio Extension and its southern recirculation using CMIP5 experiments with a high-resolution climate model MIROC4h. *Theor. Appl. Climatol.* **127**, 815–827 (2017).
- Chen, C., Wang, G., Xie, S.-P. & Liu, W. Why does global warming weaken the gulf stream but intensify the Kuroshio. *J. Clim.* **32**, 7437–7451 (2019).
- Nishikawa, H., Nishikawa, S., Ishizaki, H., Wakamatsu, T. & Ishikawa, Y. Detection of the Oyashio and Kuroshio fronts under the projected climate change in the 21st century. *Prog. Earth Planet. Sci.* **7**, <https://doi.org/10.1186/s40645-020-00342-2> (2020).
- Joh, Y. et al. Seasonal-to-decadal variability and prediction of the Kuroshio Extension in the GFDL coupled ensemble reanalysis and forecasting system. *J. Clim.* **35**, 3515–3535 (2022).
- Cai, W. et al. Butterfly effect and a self-modulating El Niño response to global warming. *Nature* **585**, 68–73 (2020).
- Cai, W. et al. Increased variability of eastern Pacific El Niño under greenhouse warming. *Nature* **564**, 201–206 (2018).
- Collins, M. et al. The impact of global warming on the tropical Pacific Ocean and El Niño. *Nat. Geosci.* **3**, 391–397 (2010).
- Romps, D. M. Response of tropical precipitation to global warming. *J. Atmos. Sci.* **68**, 123–138 (2011).
- Pendergrass, A. G., Knutti, R., Lehner, F., Deser, C. & Sanderson, B. M. Precipitation variability increases in a warmer climate. *Sci. Rep.* **7**, <https://doi.org/10.1038/s41598-017-17966-y> (2017).
- Meinshausen, M. et al. The shared socio-economic pathway (SSP) greenhouse gas concentrations and their extensions to 2500. *Geosci. Model Dev.* **13**, 3571–3605 (2020).
- Melnikova, I. et al. Carbon cycle response to temperature overshoot beyond 2 °C: an analysis of CMIP6 Models. *Earth's Future* **9**, <https://doi.org/10.1029/2020ef001967> (2021).
- Li, R., Jing, Z., Chen, Z. & Wu, L. Response of the Kuroshio Extension path state to near-term global warming in CMIP5 experiments with MIROC4h. *J. Geophys. Res.: Oceans* **122**, 2871–2883 (2017).
- Oka, E. et al. Decadal variability of Subtropical Mode Water subduction and its impact on biogeochemistry. *J. Oceanogr.* **71**, 389–400 (2015).
- Morioka, Y., Varlamov, S. & Miyazawa, Y. Role of Kuroshio Current in fish resource variability off southwest Japan. *Sci. Rep.* **9**, <https://doi.org/10.1038/s41598-019-54423-3> (2019).
- Yamamoto, A. et al. Roles of the Ocean mesoscale in the horizontal supply of mass, heat, carbon, and nutrients to the Northern Hemisphere Subtropical Gyres. *J. Geophys. Res.: Oceans* **123**, 7016–7036 (2018).
- Delworth, T. L. et al. SPEAR: The next generation GFDL Modeling System for seasonal to multidecadal prediction and projection. *J. Adv. Model. Earth Syst.* **12**, <https://doi.org/10.1029/2019ms001895> (2020).
- Kriegler, E. et al. Fossil-fueled development (SSP5): An energy and resource intensive scenario for the 21st century. *Glob. Environ. Change* **42**, 297–315 (2017).
- Riahi, K. et al. The shared socioeconomic pathways and their energy, land use, and greenhouse gas emissions implications: An overview. *Glob. Environ. Change* **42**, 153–168 (2017).
- Choi, B.-H., Kim, D.-H. & Kim, J.-W. Regional responses of climate in the northwestern Pacific Ocean to gradual global warming for a CO₂ quadrupling. *J. Meterol. Soc. Jpn.* **80**, 1427–1442 (2002).

ACKNOWLEDGEMENTS

We thank Drs. John P. Dunne and Yongfei Zhang for constructive comments on an earlier version of the manuscript. Youngji Joh received award NA18OAR4320123 under Cooperative Institute for Modeling the Earth System (CIMES) at Princeton University and the National Oceanic and Atmospheric Administration, U.S. Department of Commerce.

AUTHOR CONTRIBUTIONS

Y.J. and T.L.D. conceived the study. W.F.C. conducted the model simulations. Y.J. conducted the model output analysis, plotted figures, and wrote the paper. All authors contributed to interpreting the results and helped to improve the manuscript.

COMPETING INTERESTS

The authors declare no competing interests.

ADDITIONAL INFORMATION

Supplementary information The online version contains supplementary material available at <https://doi.org/10.1038/s41612-022-00285-z>.

Correspondence and requests for materials should be addressed to Youngji Joh.

Reprints and permission information is available at <http://www.nature.com/reprints>

Publisher's note Springer Nature remains neutral with regard to jurisdictional claims in published maps and institutional affiliations.



Open Access This article is licensed under a Creative Commons Attribution 4.0 International License, which permits use, sharing, adaptation, distribution and reproduction in any medium or format, as long as you give appropriate credit to the original author(s) and the source, provide a link to the Creative Commons license, and indicate if changes were made. The images or other third party material in this article are included in the article's Creative Commons license, unless indicated otherwise in a credit line to the material. If material is not included in the article's Creative Commons license and your intended use is not permitted by statutory regulation or exceeds the permitted use, you will need to obtain permission directly from the copyright holder. To view a copy of this license, visit <http://creativecommons.org/licenses/by/4.0/>.

© The Author(s) 2022